

Modeling chromatic instrumental effects for a better model fitting of optical interferometric data

M. Tallon^a, I. Tallon-Bosc^a, O. Chesneau^b, L. Dessart^b

^aUniversité de Lyon, Lyon, F-69003, France ; Université Lyon 1, Observatoire de Lyon, 9 avenue Charles André, Saint-Genis Laval, F-69230, France ; CNRS, UMR 5574, Centre de Recherche Astrophysique de Lyon ; Ecole Normale Supérieure de Lyon, Lyon, F-69007, France

^bUniversité de Nice Sophia-Antipolis, CNRS, UMR 7293, Laboratoire Lagrange, Observatoire de la Côte d'Azur, Boulevard de l'Observatoire, F-06300 Nice, France

ABSTRACT

Current interferometers often collect data simultaneously in many spectral channels by using dispersed fringes. Such polychromatic data provide powerful insights in various physical properties, where the observed objects show particular spectral features. Furthermore, one can measure spectral differential visibilities that do not directly depend on any calibration by a reference star. But such observations may be sensitive to instrumental artifacts that must be taken into account in order to fully exploit the polychromatic information of interferometric data. As a specimen, we consider here an observation of P Cygni with the VEGA visible combiner on CHARA interferometer. Indeed, although P Cygni is particularly well modeled by the radiative transfer code CMFGEN, we observe questionable discrepancies between expected and actual interferometric data. The problem is to determine their origin and disentangle possible instrumental effects from the astrophysical information. By using an expanded model fitting, which includes several instrumental features, we show that the differential visibilities are well explained by instrumental effects that could be otherwise attributed to the object. Although this approach leads to more reliable results, it assumes a fit specific to a particular instrument, and makes it more difficult to develop a generic model fitting independent of any instrument.

Keywords: optical interferometry, VEGA/CHARA combiner, dispersed fringes, data processing, differential visibilities, model fitting

1. INTRODUCTION

The final aim of our work is to progress on the understanding of the Luminous Blue Variable (LBV) star P Cygni by using data acquired with the VEGA visible combiner on CHARA interferometer which combines high spectral and high spatial resolution in the visible, in particular around the $H\alpha$ line. The method is based on the use of a physical model of the star as a starting point to fit the interferometric data in order to determine some physical parameters of the object.

In order to maximize the accuracy of our modeling, we have used the well known spectral features of P Cygni provided by the physical model itself as a reference to disentangle possible instrumental effects from the astrophysical information. This is the purpose of this paper.

Thus this study is focused on the modeling of the chromatic instrumental effects to determine how the instrument sees the object. P Cygni is briefly described in Section 2 along with its physical model provided by the radiative transfer code CMFGEN. Section 3 reminds some features of VEGA/CHARA and presents the data we use. Section 4 describes the model worked out from the theoretical object to the measurements. Section 5 shows the results of a fit of the differential visibilities and the squared visibilities with this extended model.

Further author information: send correspondence to Michel Tallon, E-mail: mtallon@obs.univ-lyon1.fr

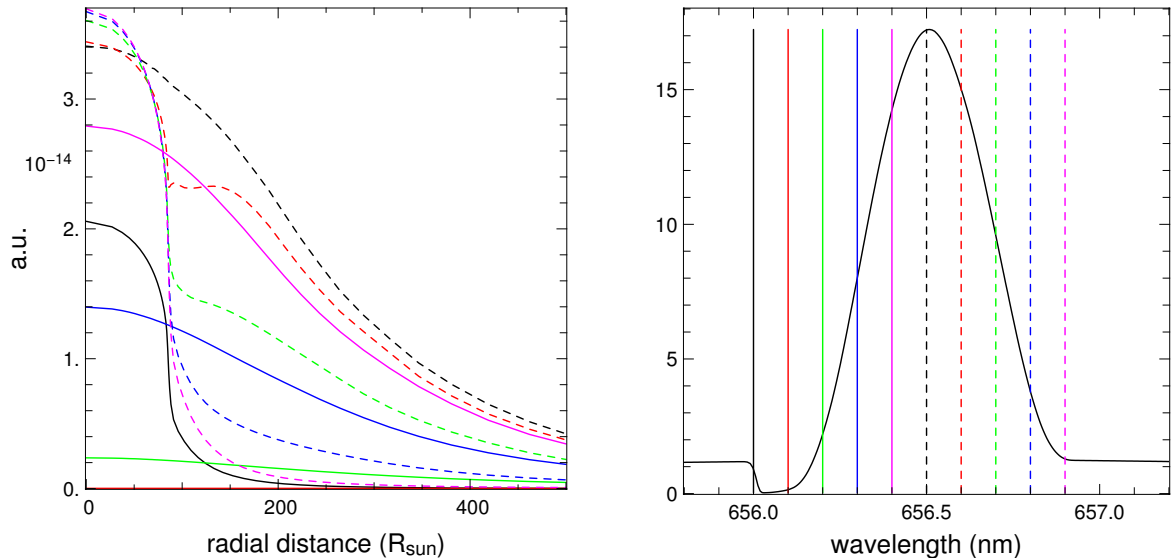


Figure 1. Samples of the theoretical radial profile of P Cygni for various positions within the $H\alpha$ spectral line. The corresponding sampled wavelengths are shown on the right. The radial profiles are integrated over 0.1 nm bandwidths.

2. P CYGNI SUMMARY AND MODELING

2.1 Synopsis of P Cygni

Hot massive stars are characterized by a stellar wind and a mass loss that affect deeply their physical properties and their fate. Time variability is ubiquitously observed in massive star, detected in photometry, spectroscopy and polarimetry at various time scales. In particular, intensive spectroscopic campaigns have provided a deep insight on the multiple aspect of the radiative wind activity observed around these massive and hot sources.

The LBV phase is a short dramatic phase that very massive stars may pass and is characterized by dense and relatively slow stellar winds. The star experiences giant eruptions in this phase that lead to the formation of circumstellar nebulae of a limited extension (≤ 5 pc). A significant fraction (about 50%) of these nebulae show -to different degrees- a bipolar structure. Such morphology may be related to the rotation of the star or by the influence of a companion.¹

The supergiant P Cygni (HD 193237, B1Ia+) is the prototype of LBV stars and its relative proximity (~ 1.7 kpc)^{2,3} represents an opportunity to observe its radiatively driven mass loss from its starting point out to the interstellar medium. The atmospheric parameters derived by Najarro et al.² revealed a helium-enriched photosphere and confirmed the high mass-loss rate and luminosity of the star.

In 1600, P Cygni experienced a giant eruption reaching the third magnitude, followed by four smaller ones which started in 1655 and terminated in 1684.⁴ The eruptions gave rise to a faint and complex nebula around the star, whose total mass is estimated to about $0.1M_{\odot}$.⁵ P Cygni is now relatively stable, but variable, with a mean V magnitude of ~ 4.8 . It is spectroscopically well observed, e.g. through AAVSO campaigns.⁶

It has also been observed by optical interferometry. At 1.7 kpc, the central star diameter corresponds to a tiny angle of 0.4 mas whilst the $H\alpha$ emitting region is much more extended due to the large mass-loss rate exhibited by this extreme star. The interferometer MIRC/CHARA provided in the H-band the first image⁷ of the extension of the wind related to this mass loss, showing it as being radially symmetrical with a FWHM of 1 mas. P Cygni was observed in the visible range too. The wind was first resolved by the Grand Interféromètre à deux télescopes (GI2T) in 1994,⁸ which estimated the extent at the $H\alpha$ and HeI 667.8 line-forming regions using a uniform-disk approximation of 5.5 ± 0.5 and 2.5 ± 2 mas, respectively. These measurements are compatible with those obtained later by the Naval Precision Optical Interferometer (NPOI) in $H\alpha$ line from 2005 to 2008.⁹ Finally, the visible spectrograph VEGA¹⁰ on CHARA observed P Cygni in this emission line as well as in HeI 667.8 and $H\beta$ lines in 2008, 2010 and 2011. This paper presents precisely a study based on some of those data.

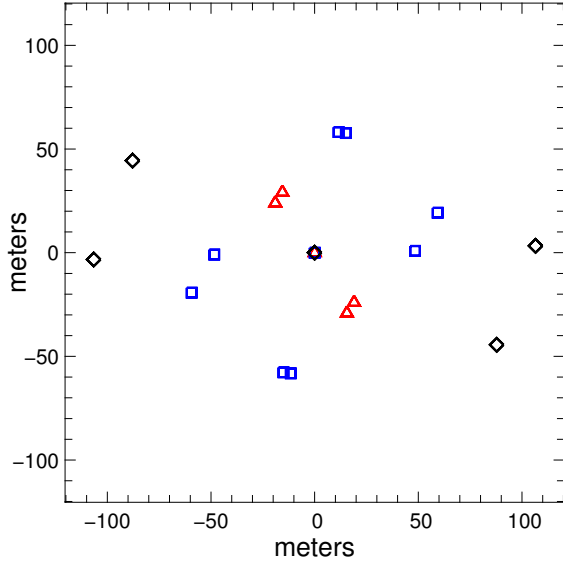


Figure 2. Baselines used for the observations, in configurations S1S2 (red triangles), E1E2 (blue squares) and W1W1 (black diamonds) of the CHARA array.

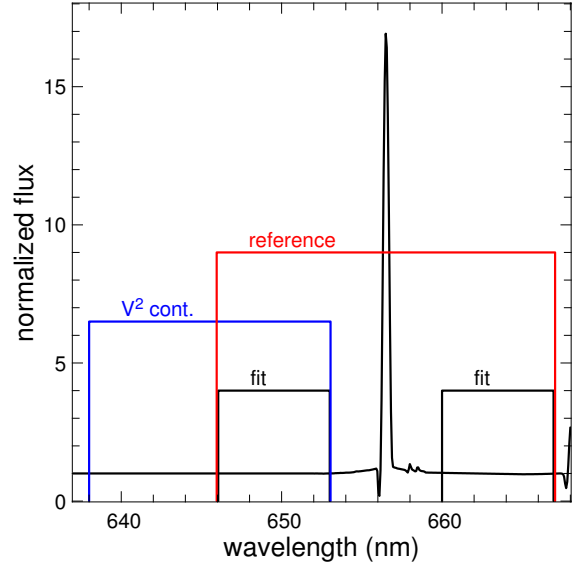


Figure 3. Theoretical PCygni spectrum from CMFGEN and definition of the bandwidths used in the text: 638–653 nm " V^2 cont." is used to compute squared visibilities in the continuum, 646–667 nm "reference" is the fixed reference bandwidth for the differential visibilities, and "fit" bandwidths are used to correct for the atmospheric piston.

2.2 CMFGEN radial profiles

The GI2T observations were performed contemporaneously with an extensive theoretical study using radiative-transfer calculations carried out with the line-blanketed non-LTE model-atmosphere CMFGEN code by Najarro et al.² This study has been improved several times.^{11–13} It solved the radiation-transfer equation for expanding media in the comoving frame, assuming spherical symmetry and steady-state, and under the constraints set by the radiative-equilibrium and statistical-equilibrium equations. It yielded the following standard fundamental parameters for PCygni, assuming the radius of the central star equal to $75 R_{\odot}$: a luminosity of $5.6 \times 10^5 L_{\odot}$, an effective temperature T_{eff} of 18200 K, a mass-loss of $3.0 \times 10^{-5} M_{\odot} \text{ yr}^{-1}$, a surface gravity $\log g$ of 1.2, and a terminal wind velocity of 185 km/s, implying a distance of 1700 ± 100 pc. Other sets of those parameters exist,² which allow to reproduce as well the real spectrum of PCygni from the UV to the IR wavelengths. But, in order to confront this theoretical model to the interferometric data, we will use the standard parameters first. The theoretical model is degenerated and interferometric data indeed must help for fixing this degeneracy as it may bring a measure of its size (see Sec. 5).

The CMFGEN code provides radial profiles for any wavelength in $H\alpha$ domain, sampled at a spectral resolution $R \sim 100000$. The corresponding spectrum is computed by integrating the profiles over the radial distance. Figure 1 shows that PCygni radial profile integrated in 0.1 nm bandwidths is rapidly changing with the wavelength in the wind-emitting region; an impact of this chromatic variations is expected on the interferometric data.

3. DATA FROM VEGA COMBINER

The interferometric data have been obtained with the instrument VEGA¹⁰ installed on CHARA¹⁴ array. VEGA is a double chambers spectrograph operating in the visible range $[0.45\text{--}0.85] \mu\text{m}$ with different possible resolutions R (1700, 5000 and 30000). Fringes are observed on the "dispersed" mode on two photon-counting detectors. In the present case, in R 5000, the $H\alpha$ region including the HeI 667.8 line has been recorded on one detector simultaneously to the $H\beta$ region on the other one. Even if some data have been recorded on PCygni in 2008 and 2011, we limit the study here to the data of summer 2010, selecting 4 files for which the temporal variability of the object may be considered as small. Each file corresponds to the record of 40000 frames with a DIT of 10ms. VEGA can combine from 2 up to 4 beams of the six 1m-telescopes of CHARA. PCygni has been successively observed with pairs of telescopes, the baselines varying from 34 to 107m, as shown by Fig. 2.

As usual with VEGA, on each data file, two types of measurements are available: (i) the squared visibilities implying a calibration with a reference star close to the object (here HD188892, 0.225 ± 0.016 mas in diameter) and (ii) the differential visibilities for relative studies between two spectral bandwidths, like, in this case, between the emitting line due to circumstellar material and the continuum due to the central star.

Figure 3 shows the bandwidths used in the data reduction software. The squared visibilities are estimated on different 15 nm bandwidths taken in the continuum parts of the spectrum. For the current study, only the blue continuum bandwidth centered at 645.5 nm is considered (Fig. 3). The differential visibilities are calculated from intercorrelations between a wide "reference" bandwidth centered on the line (here 21nm in width) and narrow ones, here 0.2 nm in width, that sample all the reference bandwidth. We only use the amplitude of the complex differential visibilities since PCygni model to confront with the data is radially symmetric. The reduction software also corrects the differential visibilities for the residual atmospheric piston by fitting a model of this effect on raw visibilities in continuum bandwidths denoted "fit" in Fig. 3.

4. MODELING FROM THE OBJECT TO THE MEASUREMENTS

4.1 Differential visibilities of VEGA

As explained in previous section, the data processing of the dispersed fringes requires several spectral bandwidths: the reference and the "fit" bandwidth. The usual estimators used for VEGA are based on two-dimensions Fourier transforms of the dispersed fringes in these bandwidths, but consider a monochromatic object observed at the central wavelength of each bandwidth.^{10,15} Since the object has strong variations versus the wavelengths, we need here to take chromatic variations of the object into account. It can be shown that taking the Fourier transform of dispersed fringes in a limited bandwidth $\{\lambda_0, \Delta\lambda_0\}$, the complex value of the energy of the fringe peak is proportional to:

$$\tilde{O}_{\Delta\lambda_0}\left(\frac{b}{\lambda_0}, \lambda_0\right) = \int_{\Delta\lambda_0} d\lambda \tilde{O}\left(\frac{b}{\lambda}, \lambda\right) \quad (1)$$

where b is the baseline. This assumes that the field of view is small compared to the width of the slit, and that the fringe spacing is approximated by a constant λ_0 in the bandwidth $\Delta\lambda_0$.

The estimator of the differential visibility for VEGA is built from a normalized cross-spectrum between a wide reference bandwidth $\{\lambda_0, \Delta\lambda_0\}$ as defined in Fig. 3, and a moving narrow (here 0.2nm in width) bandwidth $\{\lambda, \Delta\lambda\}$ scanning the full reference bandwidth:

$$V_d(u, \lambda) = \frac{\tilde{O}_{\Delta\lambda_0}(u, \lambda_0) \tilde{O}_{\Delta\lambda}^*(u, \lambda)}{\tilde{O}_{\Delta\lambda_0}(0, \lambda_0) \tilde{O}_{\Delta\lambda}^*(0, \lambda)} \quad (2)$$

where \tilde{O}^* is the complex conjugate of \tilde{O} .

Because of the jitter of the atmospheric optical path differences, this estimator is all the more attenuated as the distance between the center of the reference bandwidth and the scanning narrow bandwidth increases. This shapes $V_d(u, \lambda)$ as bell curve versus the wavelength, centered on the reference bandwidth.¹⁰ The reduction software corrects for this effect by fitting a model of the residual atmospheric piston.¹⁰ This model is here fitted in the continuum part of the spectrum, in the "fit" bandwidths as defined in Fig. 3, thus avoiding H α line.

We apply the same correction on $V_d(u, \lambda)$, but since there is no residual atmospheric piston introduced in our model, the correction is equivalent to a normalization by the average of $V_d(u, \lambda)$ in the "fit" bandwidths:

$$\hat{V}_d(u, \lambda) = \frac{V_d(u, \lambda)}{\frac{1}{\Delta\lambda_{\text{fit}}} \int_{\Delta\lambda_{\text{fit}}} d\lambda |V_d(u, \lambda)|} \quad (3)$$

We can notice that $\hat{V}_d(u, \lambda)$ can be larger than unity if the "fit" bandwidths include spectral channels with lower visibilities. In the following, we model VEGA differential visibilities by using Eq. (3).

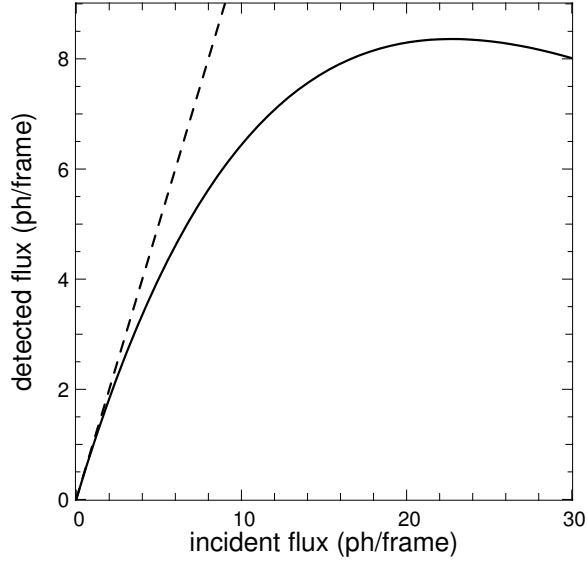


Figure 4. Saturation law of a photon counting detector (see Eq. (4)) with $\beta = 0.044$.

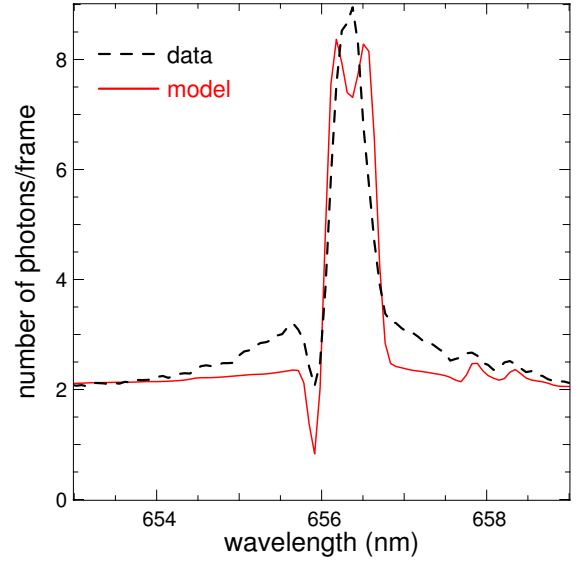


Figure 5. Fit of an observed spectrum from VEGA combiner with the theoretical CMFGEN spectrum affected by the expected model of the instrument. The model misses to reproduce the halo around the H α line.

4.2 Modeling considering the expected instrument

Our aim is to model P Cygni as seen by the instrument. Considering the strong variations of the CMFGEN model versus the wavelength (see Fig. 1), and the high photon flux in H α line, we take three known effects into account: the limited resolution of the spectrograph, a possible spectral miscalibration (fine alignment of the H α line) and a saturation of the detector.

The three corresponding parameters are determined by fitting raw spectra obtained by averaging the dispersed fringes during the data reduction process. The spectra are stored as separated fits files along usual oifits data files.¹⁶

The limited resolution of the spectrograph is modeled with a convolution versus the spectral axis by a normalized gaussian function with its FWHM as a free parameter. The model is then spectrally shifted to optimize the spectral alignment of the model with the raw spectra. Indeed, the error of the spectral calibration must be much smaller than the gaussian FWHM. Finally, a saturation of the detector is applied on the total flux in each spectral channel by using the following saturation law, suitable for photon counting detectors:¹⁷

$$\tilde{f}_d = f_i e^{-\beta f_i} \quad (4)$$

where f_i is the incident flux, \tilde{f}_d the actual detected flux, and β is a constant to be determined. This law is plotted in Fig. 4 for $\beta = 0.044$ and shows that in high flux regime, the detected flux can decrease when the incident flux yet increases.

Figure 5 shows an example representative of the fits obtained on a set of spectra. The gaussian FWHM is 0.135nm, corresponding to a spectral resolution $R=4862$ at 656.5 nm, compatible with the expected $R=5000$, the spectral shift is 0.16nm toward blue wavelengths, thus significant compared to the gaussian FWHM, and $\beta = 0.044$ for the saturation law. Nevertheless, the result is not satisfactory for two reasons. First the saturation is so strong that the shape of the modeled H α line does not match the observed one; second, the gaussian spectral PSF is unable to reproduce the observed halo around the H α line.

This last point may be critical since in this halo, the instrument can see a combination of different wavelengths of the object with very different shapes, in the continuum and in the H α line. The result of this combination depends on the relative flux in the line and in the continuum, taking the saturation of the detector into account.

Figure 6 shows the corresponding model of the differential visibilities. The object appears resolved in the continuum around the H α line, because some light from the H α line spreads in this spectral region.

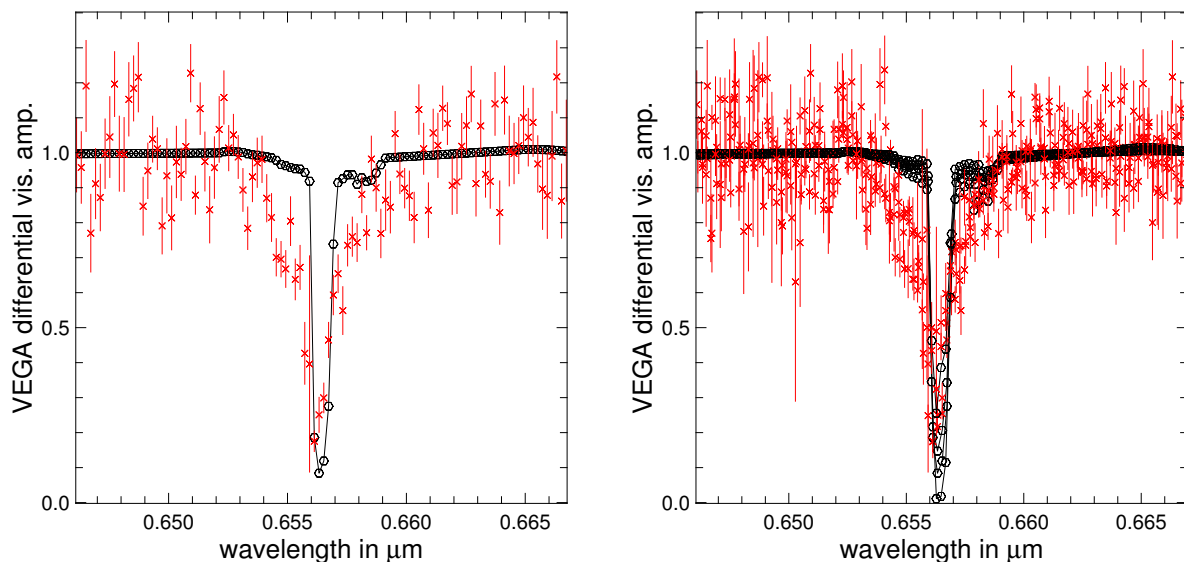


Figure 6. Fit of VEGA differential visibilities using the expected model of the instrument. Red crosses are the data; black circles are the models. On the left, comparison with the data for one single baseline. On the right, the 4 selected baselines are superimposed to present the general tendency: this model cannot explain the loss of differential visibilities around $H\alpha$ line.

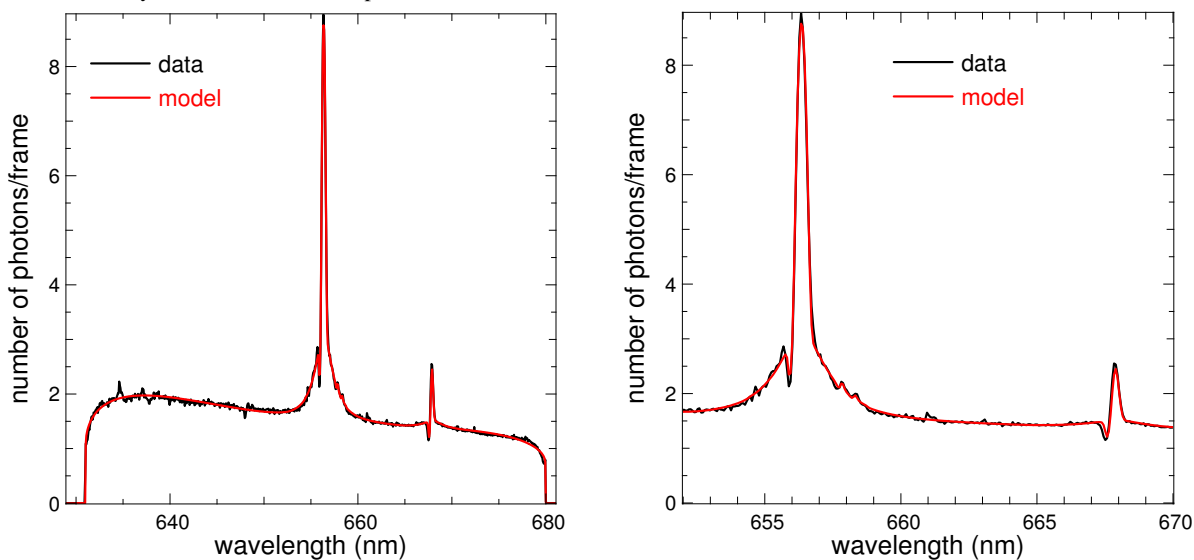


Figure 7. Example of a fit of an observed raw spectrum from VEGA combiner with the improved model of the instrument accounting for the halo of the spectral PSF. On the left, the full range of wavelengths on the detector. On the right, the same spectrum magnified on the $H\alpha$ and HeI lines.

4.3 Modeling considering the actual instrument

This section aims at the improvement of the instrumental model, essentially by refining the spectral PSF, but also taking the non-uniformity of the detector into account.

Among various models for the spectral PSF, $h(\lambda)$, a simple linear combination of a gaussian and a lorentzian function gave the best results:

$$h(\lambda) = r g(\lambda) + (1 - r) l(\lambda) \quad (5)$$

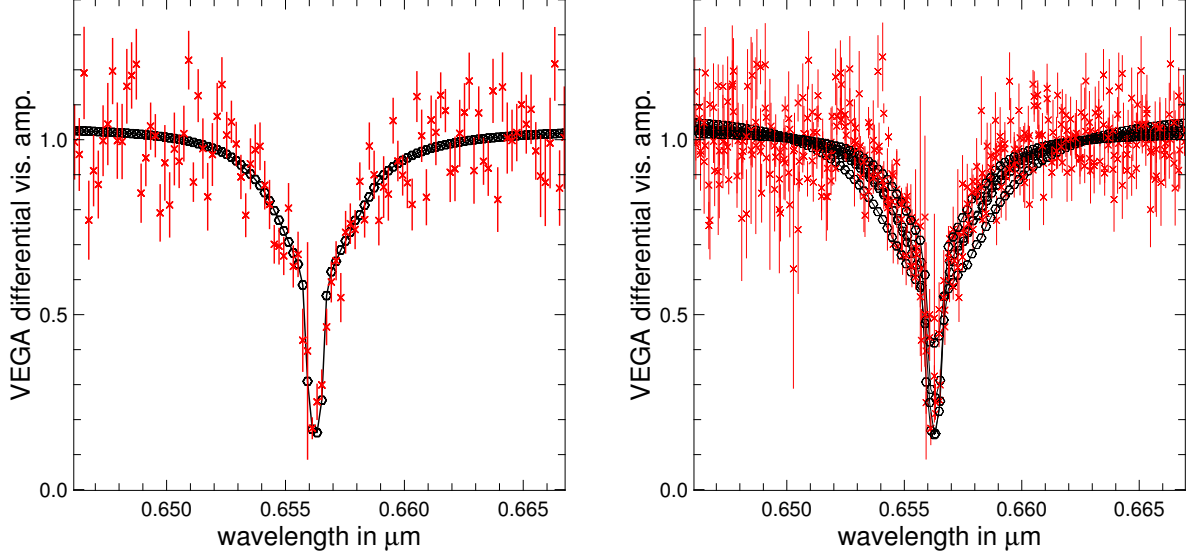


Figure 8. Alike Fig. 6, fit of VEGA differential visibilities but now using the improved model of the instrument. On the left, comparison with the data for one single baseline. On the right, the 4 selected baselines are superimposed to show the general tendency: the improved instrumental model now fully explains the loss of differential visibilities around $H\alpha$ line.

with:

$$g(\lambda) = \sqrt{\frac{\ln(16)}{\pi \Delta_g^2}} \exp\left(-\ln(16) \frac{\lambda^2}{\Delta_g^2}\right), \quad (6)$$

$$l(\lambda) = \frac{2}{\pi} \frac{\Delta_l}{\Delta_l^2 + 4\lambda^2}, \quad (7)$$

where Δ_g and Δ_l are respectively the FWHM of the gaussian and the lorentzian functions, and r is the ratio of the flux in the gaussian part of the PSF. With this writing, $g(\lambda)$, $l(\lambda)$ and $h(\lambda)$ are normalized.

The non-uniformity of the detector is modeled by a variable sensitivity of the detector as a polynomial function of the wavelength.

The result of a fit with the improved model is shown on Fig. 7. In this example, the FWHM of the lorentzian (*i.e.* the halo) is 2.1 nm and contains 60% of the flux.

The spectra associated with the other baselines give approximately the same results, with 50%–70% of the flux in the halo modeled by a lorentzian 2–3 nm in width. The variation of the results can be explained by the variation of P Cygni itself. Indeed, in this preliminary work, we have used a single model of P Cygni that corresponds to a single state of this variable star and its associated line to continuum ratio. This state may not be in agreement with our data, and furthermore, it cannot match the data acquired at different dates. Introducing a variable P Cygni model will be the next step of this work.

In the same way as in the previous section, Fig. 8 shows that the differential visibilities are now fully explained: the visibility loss of around $H\alpha$ line results from a blurring effect of the spectral PSF.

5. P CYGNI DISTANCE WITH DIFFERENTIAL VISIBILITIES

As previously stated, we only use one given state of P Cygni for now. The only free parameter that can be determined from the data is the distance of the object such that its linear size can match its observed angular size, and no other P Cygni parameter is currently adjustable.

We have implemented the model of VEGA differential visibilities in the model fitting software LITpro¹⁸ in order to fit the distance on differential visibilities only. These data are sensitive to P Cygni distance around the $H\alpha$ bandwidth where the visibilities change strongly. The value obtained is $d = 1500 \pm 120$ pc. This result is to be compared to the 1700 pc assumed by the theoretical model.

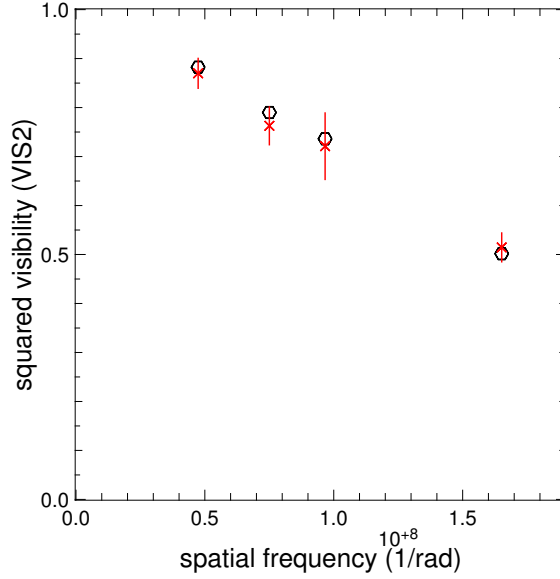


Figure 9. Best fit on the squared visibilities issued from the 4 tested baselines of Fig. 6 or Fig. 8. Red crosses are the data; black circles are the model. The resulting fitted parameter, the distance, is equal to $d = 1990 \pm 60$ pc.

On the other hand, we can also use the squared visibilities measured in the continuum bandwidth defined in Fig. 3. The squared visibilities are calibrated by a reference star, unlike the differential visibilities for which such a calibration is not necessary. These data do not depend on the circumstellar environment. The result of the fit is shown on Fig. 9, and the value obtained for the distance is $d = 1990 \pm 60$ pc.

Both results do not seem absurd when compared with the assumed theoretical value, but are not compatible with each other. The expectation is to adjust for instance the mass-loss rate to make the PCygni model compatible in both squared and differential visibilities.

6. CONCLUSION

We have shown that modeling the instrumental chromatic effects can be crucial for a reliable interpretation of interferometric data with dispersed fringes, in particular for spectral differential visibilities. In this study, by using the spectrum acquired with the interferometer itself, we were able to explain the visibility loss around the $H\alpha$ line as an instrumental effect. From this model that includes a theoretical model of PCygni, we can adjust a distance of the star from the differential visibilities only.

The next step will be to build a grid of models of PCygni with different mass-loss rates and distances, and fit these parameters. Also, we can use the other lines HeI and $H\beta$. On the instrumental side, the parameters introduced into the modeled PSF have to be confirmed with data from other type of stars.

By modeling both PCygni object and instrumental effects, the inverse problem approach used in this work does not require the data to be corrected from artifacts, but rather tries to reproduce what happens to the signal, thus avoiding for instance more correlations to be introduced in the data. Furthermore, the analysis of the residuals between the model and the data is a powerful tool to check if the model catches the dominant effects with an accuracy compatible with the measurement errors. Also the correlation between instrumental and object parameters fitted at once is a good indication of the sensitivity of the final result to instrumental parameters.

This study also shows the usefulness of the spectrum as measured from the interferometer itself. This information deserves to be stored in an upgraded version of OIFITS standard.¹⁶ This was quite useful to compute how this highly chromatic object is seen by the interferometer. As these instrumental effects depend on the combiner itself, recording a univocal identifier of the combiner in the OIFITS format would be useful, along with specific informations necessary to correctly model the data (*e.g.* reference bandwidth, bandwidth for the correction of the residual atmospheric piston).

6.1 Acknowledgments

This work is supported by the French ANR POLCA project (Processing of pOLychromatic interferometriC data for Astrophysics, ANR-10-BLAN-0511). The software used in this article has been implemented in Yorick, a free data processing language written by D. Munro (<http://sourceforge.net/projects/yorick/>).

REFERENCES

- [1] Smith, N., Li, W., Silverman, J. M., Ganeshalingam, M., and Filippenko, A. V., “Luminous blue variable eruptions and related transients: diversity of progenitors and outburst properties,” *MNRAS* **415**, 773–810 (2011).
- [2] Najarro, F., Hillier, D. J., and Stahl, O., “A spectroscopic investigation of P Cygni. I. H and HeI lines,” *Astron. Astrophys.* **326**, 1117–1134 (1997).
- [3] Lamers, H. J. G. L. M., de Groot, M., and Cassatella, A., “The distance, temperature, and luminosity of the hypergiant P Cygni (B1 IA +),” *A&A* **128**, 299–310 (1983).
- [4] de Groot, M., “On the spectrum and nature of P Cygni,” *Bull. Astron. Inst. Netherlands* **20**, 225 (1969).
- [5] Chesneau, O., Roche, M., Boccaletti, A., Abe, L., Moutou, C., Charbonnier, F., Aime, C., Lantéri, H., and Vakili, F., “Adaptive optics imaging of P Cygni in H α ,” *A&AS* **144**, 523–532 (2000).
- [6] Pollmann, E. and Bauer, T., “International Observing Campaign: Photometry and Spectroscopy of P Cygni,” *JAAVSO* **40**, 894–899 (2012).
- [7] Richardson, N. D., Schaefer, G. H., Gies, D. R., Chesneau, O., Monnier, J. D., Baron, F., Che, X., Parks, J. R., Matson, R. A., Touhami, Y., Clemens, D. P., Aldoretta, E. J., Morrison, N. D., ten Brummelaar, T. A., McAlister, H. A., Kraus, S., Ridgway, S. T., Sturmman, J., Sturmman, L., Taylor, B., Turner, N. H., Farrington, C. D., and Goldfinger, P. J., “The H-band Emitting Region of the Luminous Blue Variable P Cygni: Spectrophotometry and Interferometry of the Wind,” *ApJ* **769**, 118 (2013).
- [8] Vakili, F., Mourard, D., Bonneau, D., Morand, F., and Stee, P., “Subtle structures in the wind of P Cygni,” *A&A* **323**, 183–188 (1997).
- [9] Balan, A., Tycner, C., Zavala, R. T., Benson, J. A., Hutter, D. J., and Templeton, M., “The Spatially Resolved H α -emitting Wind Structure of P Cygni,” *AJ* **139**, 2269–2278 (2010).
- [10] Mourard, D., Clause, J.-M., Marcotto, A., Perraut, K., Tallon-Bosc, I., Bério, P., Blazit, A., Bonneau, D., Bosio, S., Bresson, Y., Chesneau, O., Delaa, O., Hénault, F., Hughes, Y., Lagarde, S., Merlin, G., Roussel, A., Spang, A., Stee, P., Tallon, M., Antonelli, P., Foy, R., Kervella, P., Petrov, R., Thiébaud, E., Vakili, F., McAlister, H., Ten Brummelaar, T., Sturmman, J., Sturmman, L., Turner, N., Farrington, C., and Goldfinger, P. J., “VEGA: Visible spECTroGraph and polArimeter for the CHARA array: principle and performance,” *Astron. Astrophys.* **508**(2), 1073–1083 (2009).
- [11] Hillier, D. J. and Miller, D. L., “The Treatment of Non-LTE Line Blanketing in Spherically Expanding Outflows,” *ApJ* **496**, 407 (1998).
- [12] Hillier, D. J., Crowther, P. A., Najarro, F., and Fullerton, A. W., “An optical and near-IR spectroscopic study of the extreme P Cygni-type supergiant HDE 316285,” *A&A* **340**, 483–496 (1998).
- [13] Dessart, L. and Hillier, D. J., “Quantitative spectroscopy of photospheric-phase type II supernovae,” *A&A* **437**, 667–685 (2005).
- [14] ten Brummelaar, T. A., McAlister, H. A., Ridgway, S. T., Bagnuolo, Jr., W. G., Turner, N. H., Sturmman, L., Sturmman, J., Berger, D. H., Ogden, C. E., Cadman, R., Hartkopf, W. I., Hopper, C. H., and Shure, M. A., “First Results from the CHARA Array. II. A Description of the Instrument,” *ApJ* **628**, 453–465 (2005).
- [15] Mourard, D., Tallon-Bosc, I., Rigal, F., Vakili, F., Bonneau, D., Morand, F., and Stee, P., “Estimation of visibility amplitude by optical long-baseline Michelson interferometry with large apertures,” *Astron. Astrophys.* **288**, 675–682 (1994).
- [16] Pauls, T. A., Young, J. S., Cotton, W. D., and Monnier, J. D., “A Data Exchange Standard for Optical (Visible/IR) Interferometry,” *PASP* **117**, 1255–1262 (2005).
- [17] Thiébaud, E., “Avoiding the photon-counting hole in speckle imaging by means of cross-correlation techniques,” *Journal of the Optical Society of America A* **14**, 122–130 (1997).
- [18] Tallon-Bosc, I., Tallon, M., Thiébaud, E., Béchet, C., Mella, G., Lafrasse, S., Chesneau, O., Domiciano de Souza, A., Duvert, G., Mourard, D., Petrov, R., and Vannier, M., “LITpro: a model fitting software for optical interferometry,” *Proc. SPIE* **7013**, 70131J (2008).